Biomaterials Science

ROYAL SOCIETY OF CHEMISTRY

PAPER

View Article Online
View Journal | View Issue

Cite this: *Biomater. Sci.*, 2021, **9**, 7603

Injectable hydrogel mediated delivery of gene-engineered adipose-derived stem cells for enhanced osteoarthritis treatment†

Wei Yu,[a] Bin Hu,‡[a] Kofi Oti Boakye-Yiadom,[a] William Ho,[b] Qijing Chen,[a] Xiaoyang Xu*[b] and Xue-Qing Zhang *[a]

Osteoarthritis (OA), a chronic and degenerative joint disease, remains a challenge in treatment due to the lack of disease-modifying therapies. As a promising therapeutic agent, adipose-derived stem cells (ADSCs) have an effective anti-inflammatory and chondroprotective paracrine effect that can be enhanced by genetic modification. Unfortunately, direct cell delivery without matrix support often results in poor viability of therapeutic cells. Herein, a hydrogel implant approach that enabled intra-articular delivery of gene-engineered ADSCs was developed for improved therapeutic outcomes in a surgically induced rat OA model. An injectable extracellular matrix (ECM)-mimicking hydrogel was prepared as the carrier for cell delivery, providing a favorable microenvironment for ADSC spreading and proliferation. The ECM-mimicking hydrogel could reduce cell death during and post injection. Additionally, ADSCs were genetically modified to overexpress transforming growth factor-β1 (TGF-β1), one of the paracrine factors that exert an anti-inflammatory and pro-anabolic effect. The gene-engineered ADSCs overexpressing TGF-β1 (T-ADSCs) had an enhanced paracrine effect on OA-like chondrocytes, which effectively decreased the expression of tumor necrosis factor-alpha and increased the expression of collagen II and aggrecan. In a surgically induced rat OA model, intra-articular injection of the T-ADSC-loaded hydrogel markedly reduced cartilage degeneration, joint inflammation, and the loss of the subchondral bone. Taken together, this study provides a potential biomaterial strategy for enhanced OA treatment by delivering the gene-engineered ADSCs within an ECM-mimicking hydrogel.

Received 14th July 2021,
Accepted 28th September 2021

DOI: 10.1039/d1bm01122g

rsc.li/biomaterials-science

Introduction

Osteoarthritis (OA) is a chronic and degenerative joint disease characterized by articular cartilage degeneration, synovitis, and subchondral bone remodeling.[1] It impairs an estimated 10% of men and 18% of women aged over 60 in the world.[2,3] However, the lack of effective disease-modifying therapies for its treatment results in the progressive development of OA, drastically affecting the life quality of patients.[4]

As a potential therapeutic agent, adipose-derived stem cells (ADSCs) have recently been extensively studied to slow down the progress of articular cartilage destruction and circumvent inflammation.[5] They perform a paracrine function by secreting large amounts of anti-inflammatory mediators and chondroprotective molecules.[6–8] Transforming growth factor-β1 (TGF-β1) is an important paracrine factor secreted by ADSCs.[9] Previous studies have confirmed that TGF-β1 facilitated the production of ECM proteins and blocked the stimulation of interleukin 1 beta (IL-1β) on chondrocytes.[10,11] Therefore, it exerts chondroprotective effects and prevents the cartilage from further damage. A recent finding also suggested that TGF-β1 could exert an anti-inflammatory effect by inducing an M2 macrophage-dominant microenvironment in the OA-affected joint.[12] Herein, the ADSCs were genetically engineered to continuously overexpress TGF-β1 to further enhance its chondroprotective and anti-inflammatory effects for OA treatment.

Delivering cells into the joint through intra-articular injection is a fairly common practice for ADSC administration. Unfortunately, direct cell injection without matrix support often results in significantly declined cell viability.[13–15] Hydrogel is a three-dimensional hydrophilic polymeric network with a reticulated structure, high water content, and adjustable mechanical properties. Therefore, hydrogels provide structural support for cells and facilitate the transport of oxygen, nutrient, waste, and soluble factors.[16,17] The inject-

[a]*Engineering Research Center of Cell & Therapeutic Antibody, Ministry of Education, and School of Pharmacy, Shanghai Jiao Tong University, Shanghai 200240, P. R. China. E-mail: xueqingzhang@sjtu.edu.cn*
[b]*Department of Chemical and Materials Engineering, New Jersey Institute of Technology, Newark, NJ 07102, USA. E-mail: xiaoyang@njit.edu*

†Electronic supplementary information (ESI) available. See DOI: 10.1039/d1bm01122g

‡These authors contributed equally.

able hydrogel has recently emerged as a promising carrier for cell delivery because it provides a minimally invasive method to deliver cells into tissues.[18–21] The injectable ECM-mimicking hydrogels with cell adhesion sites are especially attractive due to their capacities to promote cell spreading and proliferation.[16] However, the therapeutic effects of gene-engineered ADSCs coupled with an injectable ECM-mimicking hydrogel for OA treatment have not yet been investigated.

Herein, we have developed an injectable ECM-mimicking hydrogel approach that facilitates minimally invasive delivery of ADSCs overexpressing TGF-β1 (T-ADSCs) to improve the therapeutic outcomes of OA treatment (Fig. 1). The *in situ* formed hydrogel implant is degradable and biocompatible with tunable physical properties, which provides a favorable 3-dimensional (3D) environment for cell growth, leading to improved cell retention and survival and a long-lasting expression of the therapeutic protein TGF-β1. *In vitro* 3D culture and cell injection experiments were conducted to evaluate the cytocompatibility and cell protection potential of the hydrogel. The ADSCs were transfected with a plasmid encoding TGF-β1 to overexpress the TGF-β1 protein. The paracrine protective effect of the T-ADSCs was evaluated in a co-culture system. The *in vivo* therapeutic effects of the developed combinatorial therapy were investigated through micro-computed tomography (micro-CT) and histological analysis. Noteworthily, this hydrogel-mediated drug delivery approach coupled with gene-engineered cell therapy could be easily tuned for other biomedical applications of interest, providing great potential for future clinical practices and treatments.

Materials and methods

Materials

Hyaluronic acid (HA, M_w = 100 kDa) was purchased from Bloomage Freda Biopharm Co., Ltd (Shandong, China). 1,4-Butanediol diacrylate, 4-amino-1-butanol, and 1-(3-aminopropyl)-4-methyl piperazine were purchased from Sigma-Aldrich (Shanghai, China). Other chemical reagents were purchased from Aladdin (Shanghai, China). Rat tail Col I was purchased from BD BioCoat. Dulbecco's modified Eagle's medium/Ham's F-12 medium (DMEM/F12), fetal bovine serum (FBS), penicillin (Pen), and streptomycin (Strep) were purchased from Gibco (Shanghai, China). CD90 and CD45 antibodies were purchased from BioLegend (San Diego, CA). Safranin O/Fast Green staining solution, hematoxylin, and eosin were purchased from Servicebio Technology Co., Ltd (Wuhan, China).

Synthesis and characterization of thiolated hyaluronic acid (HA-SH)

HA-SH was synthesized according to a previously described method with slight modifications.[22] Briefly, HA (1 g) was dissolved in deionized water (DI-H_2O, 100 mL) and the pH was adjusted to 5.5. *N*-(3-dimethylaminopropyl)-*N*′-ethyl carbodiimide hydrochloride (1.22 g) was added to the resultant solution and this reaction process occurred for 30 min. Subsequently, *N*-hydroxysuccinimide (0.73 g) and cysteamine hydrochloride (1.16 g) were added to the reaction mixture and the reaction process was sustained for another 4 h while adjusting the pH in the range of 4.75–5.0. The final reaction solution was transferred into dialysis tubes (3.5 kDa) and dialyzed against DI-H_2O (pH = 3.5) containing 0.1 M NaCl for 48 h and then dialyzed against DI-H_2O for another 24 h (pH = 3.5). The purified solution was lyophilized to yield the HA-SH polymer. ^{1}H NMR spectra of HA-SH and HA were recorded on an Agilent 400 MHz NMR spectrometer.

Preparation of the hydrogels

Either the Col I solution (1.3 mg mL^{-1}, 550 μL) or 1× PBS (550 μL) was used to dissolve a certain amount of HA-SH polymer. The pH of the solution was adjusted to 7.8 using 1 N NaOH, and a certain amount of 1× PBS was added to get a

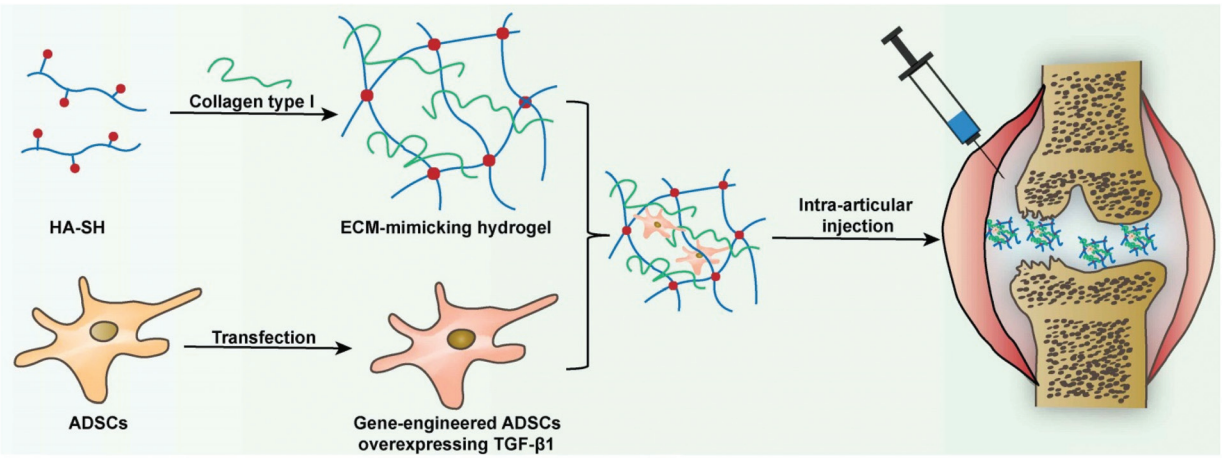

Fig. 1 A schematic demonstration of the experimental design. An injectable ECM-mimicking hydrogel was prepared *via* self-crosslinking of thiolated hyaluronic acid (HA-SH) and self-assembly of collagen type I (Col I). The gene-engineered ADSCs overexpressing TGF-β1 were encapsulated in the prepared hydrogel and delivered into the knee joint of the rat OA model for OA treatment.

final volume of 600 μL. Finally, the mixed solution was transferred into a cylindrical Teflon mold with different diameters (8 mm or 24 mm) to form the hydrogels.

Swelling test

The hydrogel disks (diameter = 8 mm and height = 1.5 mm) were incubated in PBS (7.4) for 24 h at 37 °C. The swollen hydrogels were accurately weighed (W_t) after the excess amount of water was removed from the washed gels (DI-H_2O, 3× washing) using filter paper. The hydrogel samples were lyophilized to determine the dried weight (W_0). The swelling ratio (Q_m) was calculated by comparing the initial weight (W_t) with the dried hydrogel weight (W_0) as shown below (n = 3):

$$Q_m = W_t/W_0. \quad (1)$$

Degradation test

The hydrogel disks (diameter = 8 mm and height = 1.5 mm) were lyophilized and the initial weight (W_0) was recorded. The dried hydrogel disks were immersed in PBS (7.4) with or without 50 U mL^{-1} hyaluronidases (Yeasen, China) and shaken at a speed of 200 rpm min^{-1} at 37 °C in a mechanical shaker (Zhichu ZQZY-CF, China). At pre-established time points, the hydrogel disks were removed from incubation, washed with DI-H_2O, and lyophilized to obtain the weight of dried gels (W_t). Hydrogel weight loss was calculated according to the formula below (n = 3):

$$\text{Weight loss } (\%) = [(W_0 - W_t)/W_0] \times 100\%. \quad (2)$$

Rheological test of the hydrogels

Kinexus ultra+ rheometer (Malvern, UK) was used to test the mechanical properties of hydrogels. The prepared hydrogels were placed on a 25 mm parallel plate with a gap of 500–750 μm to run the stress and frequency sweeps under a controlled stress of 1 Pa (n = 3) at 37 °C. The shear-thinning properties of the HA-Col hydrogel were characterized by measuring linear viscosity (η) under a time sweep mode at 37 °C.

Isolation and characterization of ADSCs

All experiments involving primary cell extraction were conducted under approved animal welfare protocols (Institutional Animal Care and Use Committee, Shanghai Jiao Tong University). ADSCs were isolated from inguinal regions of the adipose tissue of the rats.[23] The morphology of ADSCs was imaged using an inverted phase microscope after staining (Olympus). Flow cytometry (BD Fortessa) was used to identify the surface biomarkers of ADSCs. The differentiation potential of ADSCs was evaluated in adipogenic, osteogenic, and chondrogenic induced culture media (Saiye Biotechnology, China). ADSCs passaged for the third time were used in the following experiments.

3D culture of ADSCs

ADSC suspension was mixed with HA-SH and Col I solutions to obtain a final concentration of 1×10^6 cells per mL cell–hydrogel constructs. They were transferred into a 24-well plate and DMEM/F12 supplemented with 10% FBS and 1% Pen/Strep were added. At days 1, 3 and 5, the ADSC morphology in the different cell-hydrogel constructs was imaged using an inverted phase microscope. The viability of ADSCs encapsulated in the hydrogel was evaluated by live/dead staining (Dalian Meilun, China), and the cell–hydrogel construct was harvested after 3 days of 3D culture and stained with 2×10^{-3} M calcein acetoxymethyl ester (calcein AM) and 8×10^{-3} M pyridine iodide (PI) in PBS for 30 min. Then it was imaged using a confocal microscope (Leica).

Evaluation of the protective effect of the 2-HA-Col hydrogel on cells

The cell–hydrogel construct was transferred into a syringe, which was then excluded from a 25-gauge needle. The confocal dish was used to collect the excluded cell–hydrogel construct. A small amount of the medium was added and incubated at 37 °C with 5% CO_2 for 1 h, followed by live/dead staining. Fluorescence images were taken using a confocal microscope. ADSCs suspended in 1× PBS served as the control. The viability of cells in the 2-HA-Col hydrogel was calculated using ImageJ software (n = 3).

SEM characterization

The sectional surface of the dried 2-HA-Col hydrogel or cell–hydrogel construct harvested after 1 day of 3D culture was coated with a layer of 5 nm gold (EM ACE600, Leica). The microstructure of the 2-HA-Col hydrogel or cell morphology in the 2-HA-Col hydrogel was observed by SEM (MIRA3, TESCAN). The average pore size of the 2-HA-Col hydrogel was calculated using ImageJ software (n = 3).

Gene transfection

P2A, a cleavable 2A peptide sequence,[24] was cloned into the pcDNA3.1(+) plasmid between the enhanced green fluorescent protein (*egfp*) gene and *tgf-β1* gene (pEGFP-TGF-β1, GENEWIZ, China). Poly(β-amino ester) (PBAE) was synthesized and used as the pEGFP-TGF-β1 delivery carrier.[25] The optimal ratio of PBAE to pEGFP-TGF-β1 was determined by an agarose gel retardation assay. The mean size and zeta potential of the PBAE/pEGFP-TGF-β1 nanocomplexes were determined by using a dynamic light scattering spectrophotometer (Malvern, UK). For cell transfection, ADSCs (6×10^4 cells per well) were seeded in a 24-well plate. After 12 h, the ADSCs were treated with serum-free DMEM/F12 containing different PBAE/pEGFP-TGF-β1 nanocomplexes (2 μg pEGFP-TGF-β1 for each well). The PEAE/pEGFP-TGF-β1 nanocomplexes were removed and replaced with fresh culture medium after 4 h of incubation. The expression of EGFP in cells was imaged using a fluorescence microscope (Olympus), and the transfection efficiencies were determined by flow cytometry after 24 h of

transfection (n = 3). Non-transfected ADSCs were used as controls.

Cell viability test

A cell counting kit-8 (CCK-8) assay (Beyotime, China) was used to evaluate the toxicity of different nanocomplex formulations. ADSCs were seeded into 96 wells at a density of 5×10^3 per well for the cell toxicity assay and a density of 2×10^3 per well for the cell proliferation test. Cells were transfected (0.32 μg pEGFP-TGF-β1 for each well) using the method described above. At predetermined time points, the cell viability was examined according to the manufacturer's instructions (n = 3). Non-transfected ADSCs were used as controls.

Preparation and characterization of T-ADSCs

ADSCs (2.5×10^4 cells per well) were seeded in a 24-well plate. After 12 h, the cells were transfected using the optimal nanocomplex formulation. The expression of EGFP in the cells was assessed using a fluorescence microscope, and the transfection efficiencies were determined by flow cytometry. The cell culture supernatant was collected at each defined time point and it was replaced with a fresh medium every two days. ELISA (Neobioscience, China) test was performed to quantify the concentration of TGF-β1 in the culture supernatants of T-ADSCs (n = 3). The supernatants of non-transfected ADSCs were used as controls.

Co-culture of ADSCs and chondrocytes

Primary chondrocytes were isolated from the knee joint cartilage of the rats.[26] Chondrocytes were identified by immunocytochemistry of collagen type II (Col II).[27] Chondrocytes that were passaged for the first time were used in all experiments.

Chondrocytes (2.5×10^4 cells per well) were seeded in six-well plates or cell culture inserts (0.4 μm pores, BD Falcon™), and ADSCs (2.5×10^4 cells per insert) were seeded in cell culture inserts, both containing DMEM/F12 supplemented with 10% FBS and 1% Pen/Strep. After 12 h, the ADSCs were transfected with PBAE/pEGFP-TGF-β1 nanocomplexes. Then after another 12 h, the co-culture systems were established between T-ADSCs, ADSCs, and chondrocytes in the cell culture inserts and chondrocytes in six-well plates as described below: (1, control) chondrocytes (well) and chondrocytes (insert); (2, IL-1β) chondrocytes (well) and chondrocytes (insert); (3, IL-1β + ADSCs) chondrocytes (well) and ADSCs (insert); (4, IL-1β + T-ADSCs) chondrocytes (well) and T-ADSCs (insert). The control group was cultured in DMEM/F12 supplemented with 10% FBS and 1% Pen/Strep. On the other hand, the culture medium of the other groups was supplemented with 10 ng mL^{-1} IL-1β (Neobioscience, China) to stimulate the isolated chondrocytes to mimic OA chondrocytes.[28] After 3 days of co-culture, the total RNA of the chondrocytes in the well was extracted and analyzed using quantitative reverse transcription PCR (qRT-PCR). The primer sequences for the qRT-PCR are listed in Table S1.† All the values were normalized and compared to GAPDH (n = 3).

Surgically induced rat OA model

Male Sprague-Dawley (SD) rats (180–200 g, 7 weeks old) were purchased from Shanghai SLAC Laboratory Animal Co., Ltd. The rats were housed in a specific pathogen-free environment in the animal center of Shanghai Jiao Tong University. All surgical and care procedures were reviewed and approved by the Institutional Animal Care and Use Committee (Shanghai Jiao Tong University).

A week later, OA was surgically induced on the right knee of the rat by anterior cruciate ligament transection and partial medial meniscectomy (ACLT/MMx).[29] Briefly, the rats were anesthetized with 1% pentobarbital sodium (40 mg kg^{-1}). The right hindlimb was shaved and disinfected with iodophor. Two incisions (0.5–1 cm) were made with a #11 scalpel on the skin and joint capsule until the patella could be subluxated laterally, exposing the joint. The ACL was exposed and transected with microscissors, and the anterior drawer test was conducted to confirm the transection. Subsequently, the medial meniscus was partially transected with a #11 blade and carefully taken out with tweezers. After the completion of the procedure, the patella was relocated. The joint capsule was closed with a 5-0 resorbable suture, while the skin was closed with a 4-0 normal suture. After surgery, rats were given penicillin sodium to prevent surgery-associated infections.

4 weeks post-surgery, the rats were divided into 5 groups (n = 5 per group): PBS (40 μL), ADSCs (2×10^5 cells in 40 μL PBS), T-ADSCs (2×10^5 cells in 40 μL PBS), gel + ADSCs (2×10^5 cells in 40 μL gel) and gel + T-ADSCs (2×10^5 cells in 40 μL gel). The rats treated with the sham surgery were used as control (sham, n = 5). The T-ADSCs and cell-loaded hydrogel were prepared following the methods described above. Treatments were administered by intra-articular injection into the affected joint on the 4th and 6th week after surgery.

Quantitation of tumor necrosis factor-alpha (TNF-α) concentration in the synovial fluid

Rats were sacrificed after 4 weeks of intra-articular injection. The joint cavity was flushed with 40 μL of cold 1× PBS (pH = 7.4), and about 20 μL of diluted synovial fluid was carefully collected for each rat. The collected samples were centrifuged at 1×10^4 rpm min^{-1} for 10 min and stored at −80 °C prior to ELISA analysis. The TNF-α concentration in the synovial fluid was determined by ELISA (Neobioscience, China).

Micro-CT scanning

The knee joints of three rats were randomly chosen from each group and imaged in a micro-computed tomography scanner (VENUS micro-CT, PINGSENG, China). Scanning was performed using 90 kV voltage and 0.07 mA current. 3D reconstruction of CT image datasets and analysis of the regions of interest (ROI) of trabecular bone were performed using an image processing software (VENUS, PINGSENG, China).

Histological analysis

The knee joints were decalcified in 10% ethylenediaminetetraacetic acid for 5 weeks and it was changed every two days. Decalcified bone tissues were embedded in paraffin wax, cut into 5 nm sections, and stained with hematoxylin/eosin (H&E), Safranin O (4% w/v) or Fast Green (0.1% w/v). Primary antibodies against Col II (Servicebio, 1 : 200) were used for immunohistochemical staining to observe the expression of Col II in the cartilage. The cartilage lesions were graded using two blinded graders, using the modified Mankin scale,[30] and the sections of the synovial joint tissue were scored for three features, according to Krenn: inflammatory infiltrates, synovial stroma and lining cell hyperplasia.[31]

Statistical analysis

All values were presented as mean ± standard deviation. Statistical comparison was performed using Student's *t*-test, using GraphPad Prism 8. A *p*-value <0.05 was considered statistically significant (*). **, ***, and **** represent $p < 0.01$, $p < 0.001$, and $p < 0.0001$. $p > 0.05$ was not significant (ns).

Results

Synthesis and characterization of HA-SH

The modification of HA resulted in the new resonant peaks in the ^{1}H NMR spectra at 2.52 ppm and 2.31 ppm (Fig. S1, ESI†), corresponding to the methylene protons of $-CH_2CH_2SH$ groups.[32] The amount of the thiol groups conjugated on the HA backbone was 3.98×10^{-4} mol g^{-1}, determined by Ellman's assay.[33]

Sol-to-gel transition

The hydrogel formulations are listed in Fig. 2A. The precursor solution of the hydrogel turned into a gel with its pH adjusted to 7.8 (Fig. 2B). Rapid sol-to-gel transitions were observed within 6 minutes for all the hydrogel formulations, determined by an invert-flow test (Fig. 2C).[34]

Swelling and degradation

The swelling ratio of HA hydrogels formed through the cross-linking of HA-SH reduced with the increase of the HA-SH mass fraction, in the range of 50.2 to 76.2 (Fig. 2D). When Col I was incorporated into the HA hydrogels, the swelling ratio of hydrogels significantly decreased by 21.1%, 26.4, and 38.2%

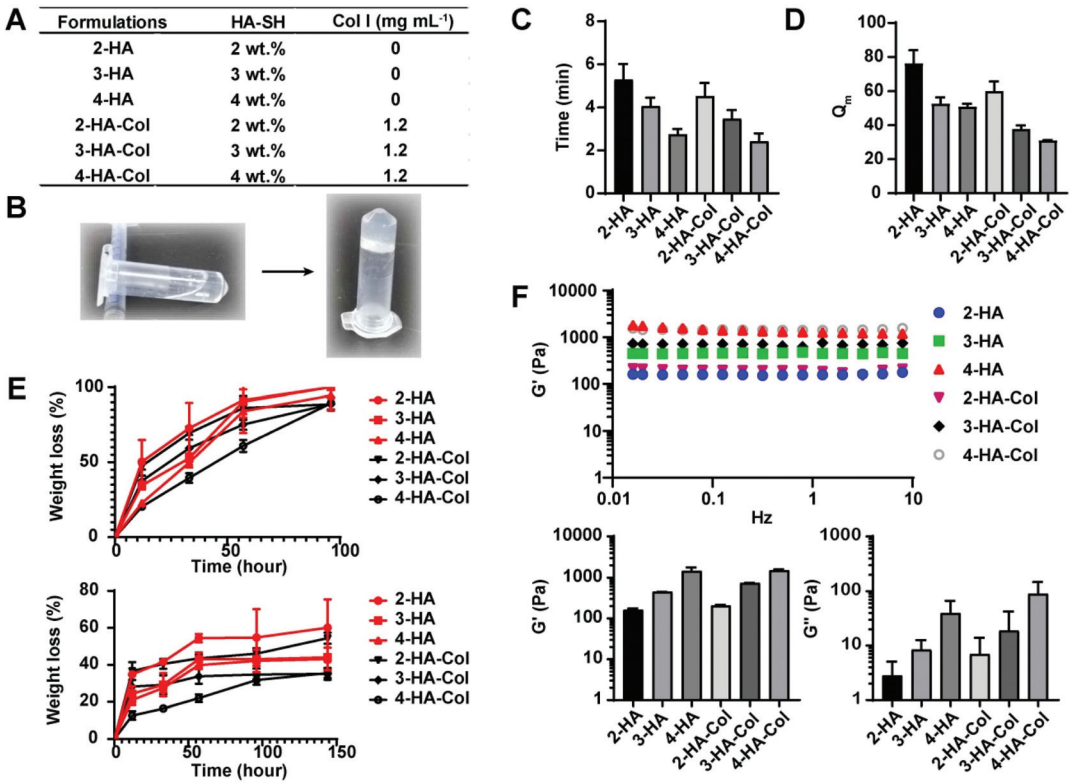

Fig. 2 Characterization of the different hydrogel formulations. (A) Formulation of different hydrogels. (B) The representative photographs of the sol-to-gel transition of the hydrogel. (C) Time needed for the sol-to-gel transition of the hydrogels, $n = 3$. (D) Swelling ratio (Q_m) of various hydrogel formulations $n = 3$. (E) *In vitro* degradation of hydrogels in PBS with (top) or without (bottom) 50 U mL^{-1} hyaluronidases at 37 °C, $n = 3$. (F) Representative curves of storage modulus (G') of various hydrogel formulations (top). Statistics of G' and loss modulus (G'') of various hydrogel formulations (bottom). Rheological frequency sweep performed with the controlled stress of 1 Pa, $n = 3$. Data are presented as the mean ± standard deviation ($n = 3$).

for hydrogels termed 2-HA-Col, 3-HA-Col, and 4-HA-Col, respectively. When incubated in PBS containing 50 U mL^{-1} hyaluronidases, 2-HA was completely degraded in 4 days, and the other hydrogels remained less than 12% of their weights (Fig. 2E). However, the hydrogels exhibited a much slower degradation rate in PBS, where only an approximate weight of 60% was degraded for the 2-HA hydrogel on day 6. And the incorporation of Col I slowed down the degradation of the hydrogels in all cases.

Rheological properties

The hydrogel exhibited a linear viscoelastic behavior when the shear stress was in the range of 0.1 Pa to 10 Pa (Fig. S2†), and a shear stress of 1 Pa was selected for subsequent sweeps. As shown in Fig. 2F, the storage modulus (G') and loss modulus (G'') of the hydrogels increased with an increase in the HA-SH mass fraction. The G' of the yielded HA hydrogels varied from 162.5 Pa to 1453.3 Pa. The addition of Col I further improved the G' and G'' values of the hydrogels. The G' of 2-HA-Col, 3-HA-Col, and 4-HA-Col hydrogels increased by 27.0%, 63.8%, and 3.6%, respectively, when compared with their corresponding HA hydrogels, while no difference was observed in G'' before and after the addition of Col I. It is worth noting that the HA-Col hydrogel displayed a shear-thinning behavior that is desirable for cell delivery through injection (Fig. S3, ESI†).[35] The viscosity of the hydrogel decreased from 137.2 Pa.s to 36.07 Pa.s with an increase in the shear rate.

3D culture of ADSCs

ADSCs were isolated from the rat inguinal adipose tissue. As shown in Fig. S4A,† the isolated cells exhibited a fibroblast-like morphology. Phenotypic analysis *via* flow cytometry indicated that the isolated cells were positive for the mesenchymal stem cell marker CD90 and negative for the hematopoietic lineage marker CD45 (Fig. S4B and S4C†).[36] When cultured in the induced medium, the isolated cells differentiated toward the adipogenic, osteogenic, or chondrogenic lineage, showing the typical characteristics of ADSCs (Fig. S4D–F†).[37]

The ADSCs were encapsulated in the hydrogels for the 3D culture. The ADSCs in the 2-HA-Col and 3-HA-Col hydrogels started to spread and form protrusions at day 1 (Fig. 3A). However, the cells in the 4-HA-Col hydrogel maintained a spherical morphology without spreading over time. On days 3 and 5, the cells in the 2-HA-Col and 3-HA-Col hydrogel matrices exhibited a more elongated morphology and formed interconnected networks. Among the three hydrogels tested, the 2-HA-Col hydrogel provided considerable benefits through promoting cell spreading and proliferation as shown in Fig. 3A. The live/dead staining of ADSCs after 3 days of culture in the 2-HA-Col hydrogel demonstrated that most of the cells were viable with a spread morphology in the hydrogel matrix (Fig. 3B and S5, ESI†). Based on these results, the 2-HA-Col hydrogel was selected as the carrier for cell delivery.

SEM

The 2-HA-Col hydrogel had a porous microstructure with an average pore size of 74.4 ± 10.0 μm (Fig. 3C). The attachment of ADSCs on the 2-HA-Col hydrogel was also observed by SEM. They exhibited an elongated morphology in the hydrogel matrix, which was consistent with the finding of the 3D culture (Fig. 3D).

Cell-protective effect of the 2-HA-Col hydrogel

The cell–hydrogel construct was injected through a 25-gauge needle and subjected to live/dead staining 1 h post-injection. As shown in Fig. 3E, the injection of ADSCs within the 2-HA-Col hydrogel led to obviously lower cell death than the injection of the cell–PBS suspension. Specifically, more than 97% of the cells remained alive when administered using the hydrogel as the cell carrier (Fig. 3F).

Preparation and characterization of T-ADSCs

Different PBAE/pEGFP-TGF-β1 nanocomplex formulations were prepared and characterized (Fig. S6, ESI†). The PBAE/pEGFP-TGF-β1 nanocomplex formulated at a weight ratio of 60/1 was selected as the gene transfection agent for the preparation of T-ADSCs considering both transfection efficiency and cell toxicity (Fig. S7, ESI†). The long-lasting expression of EGFP was exhilaratingly observed in T-ADSCs. The proportion of EGFP positive cells peaked at 52.8%, 48 h post-transfection, after which it started to decrease, leading to the decline in the EGFP fluorescence intensity (Fig. 4A and B). Noteworthily, 20% of the cells were still EGFP positive even 5 days post-transfection.

Meanwhile, the ADSCs were able to continually express TGF-β1 after transfection. The cumulative expression of TGF-β1 in T-ADSCs was 34.3% higher than that of the non-transfected ADSCs even 5 days post-transfection (Fig. 4C). No obvious toxicity was observed during the 5 days of transfection *via* the cell proliferation test, which indicated the excellent cytocompatibility of the optimal PBAE/pEGFP-TGF-β1 nanocomplexes (Fig. 4D).

The enhanced paracrine effect on the OA-like chondrocytes of T-ADSCs

Chondrocytes were isolated from the knee joint of the rat. As shown in Fig. S8,† the isolated cells formed stretched, polygonal-shaped pseudopodia after culture and expressed the typical biomarker of chondrocytes, Col II.

The chondrocytes were co-cultured with ADSCs, or T-ADSCs in transwells for 3 days, followed by extraction of the total RNA of the chondrocytes in the wells for qRT-PCR analysis (Fig. 4E). As shown in Fig. 4F, the addition of IL-1β resulted in a significant decrease in the levels of Col II and aggrecan (Agg) mRNA by 94.0% and 96.0%, respectively, and an increase by 166.3-fold in the level of TNF-α mRNA compared to that of the control group (without the addition of IL-1β). The levels of Col II and Agg mRNA showed no statistical significance between the IL-1β + ADSC group and the IL-1β group. However, the

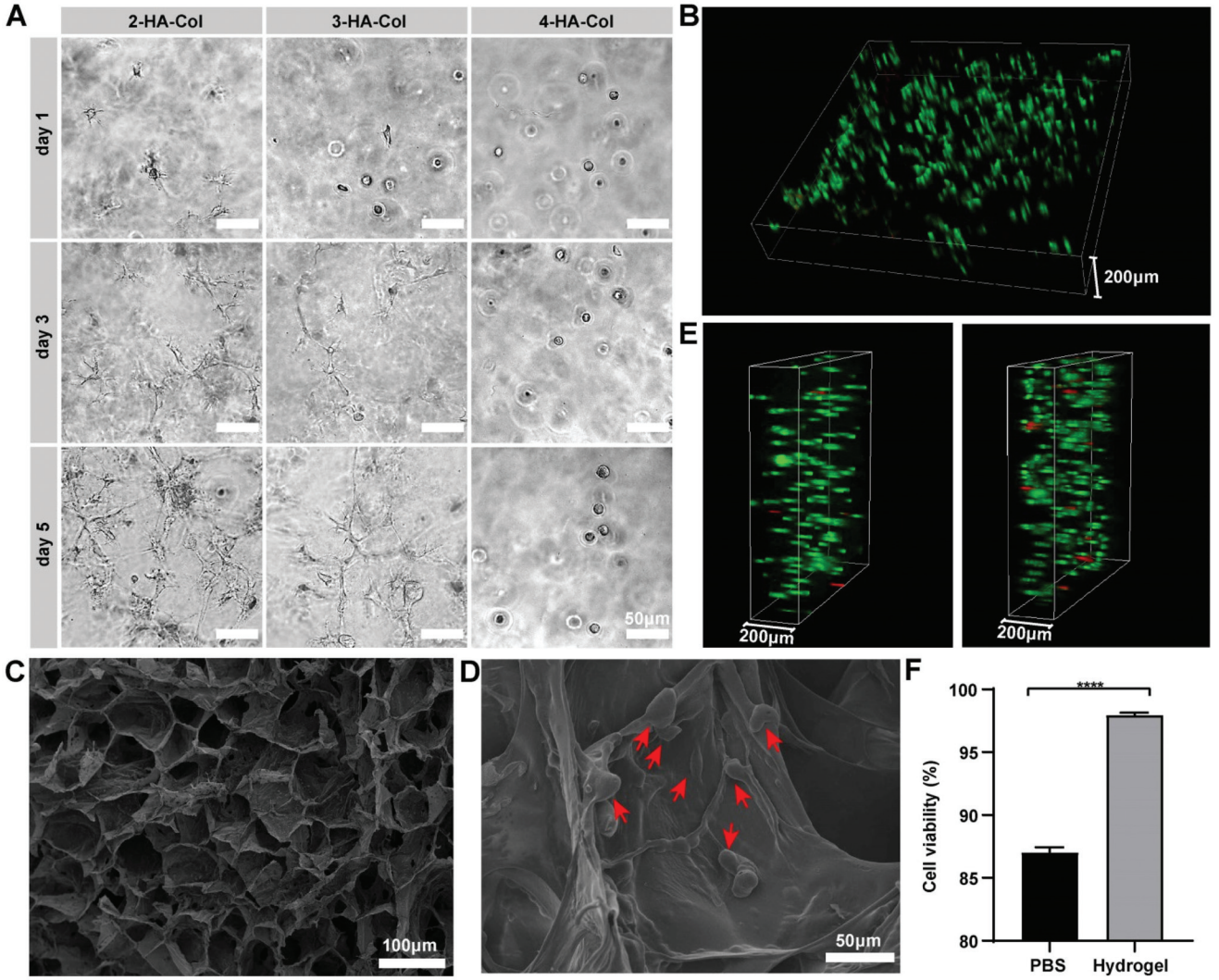

Fig. 3 Evaluation of the cytocompatibility and protective potential of the HA-Col hydrogel. (A) Morphology of ADSCs encapsulated in different hydrogel formulations on days 1, 3, and 5 of cell culture. (B) Live/dead staining images of ADSCs encapsulated in 2-HA-Col after 3 days of 3D culture, where calcein AM stained live cells green and PI stained dead cells red. (C) SEM image of the 2-HA-Col hydrogel. (D) SEM image indicated the cell morphology (red arrows) when encapsulated in the 2-HA-Col hydrogel after 1 day of 3D culture. (E) Live/dead staining images of ADSCs 1 h post-injection within 2-HA-Col (left) and PBS (right). The injection was performed using a 25-gauge needle with an inner diameter of 0.5 mm. (F) Quantification of the viability of ADSCs in PBS and 2-HA-Col hydrogel 1 h post-injection. Data are presented as the mean ± standard deviation (n = 3), ****p < 0.0001.

mRNA levels of Col II and Agg were 3.268-fold and 1.934-fold higher in the IL-1β + T-ADSC group than in the IL-1β group, respectively, indicating that ADSCs were imparted with the enhanced paracrine effects following gene modification. Besides, the TNF-α mRNA level was downregulated by 83.06% and 69.56% in the IL-1β + T-ADSC and IL-1β + ADSC groups, respectively, which highlighted the enhanced therapeutic effects of T-ADSCs.

Chondroprotective effect of the T-ADSC-loaded hydrogel

The rat OA model was established by ACLT/MMx surgery (Fig. S9, ESI†). PBS, ADSCs, T-ADSCs, ADSC-loaded hydrogels, or T-ADSC-loaded hydrogels were injected into the affected joint of the rats 4 and 6 weeks post-surgery (Fig. 5A). By analyzing the gross appearance of the femurs, the cartilage was found to be eroded and worn out (red frame) following PBS treatment, showing the typical degenerative changes of OA (Fig. 5B). Compared with the PBS control group, these symptoms were alleviated after treatment with ADSCs, T-ADSCs, ADSC-loaded hydrogels, or T-ADSC-loaded hydrogels. The safranin O/fast green staining revealed the decrease in the proteoglycan (red) content in the PBS group (Fig. 5C). But alleviated degenerative feature was observed in the cells or cell-loaded hydrogel treatment groups. A higher content of proteoglycans was also generated in these groups, where the Gel + T-ADSC group displayed the highest level of proteoglycans. Col

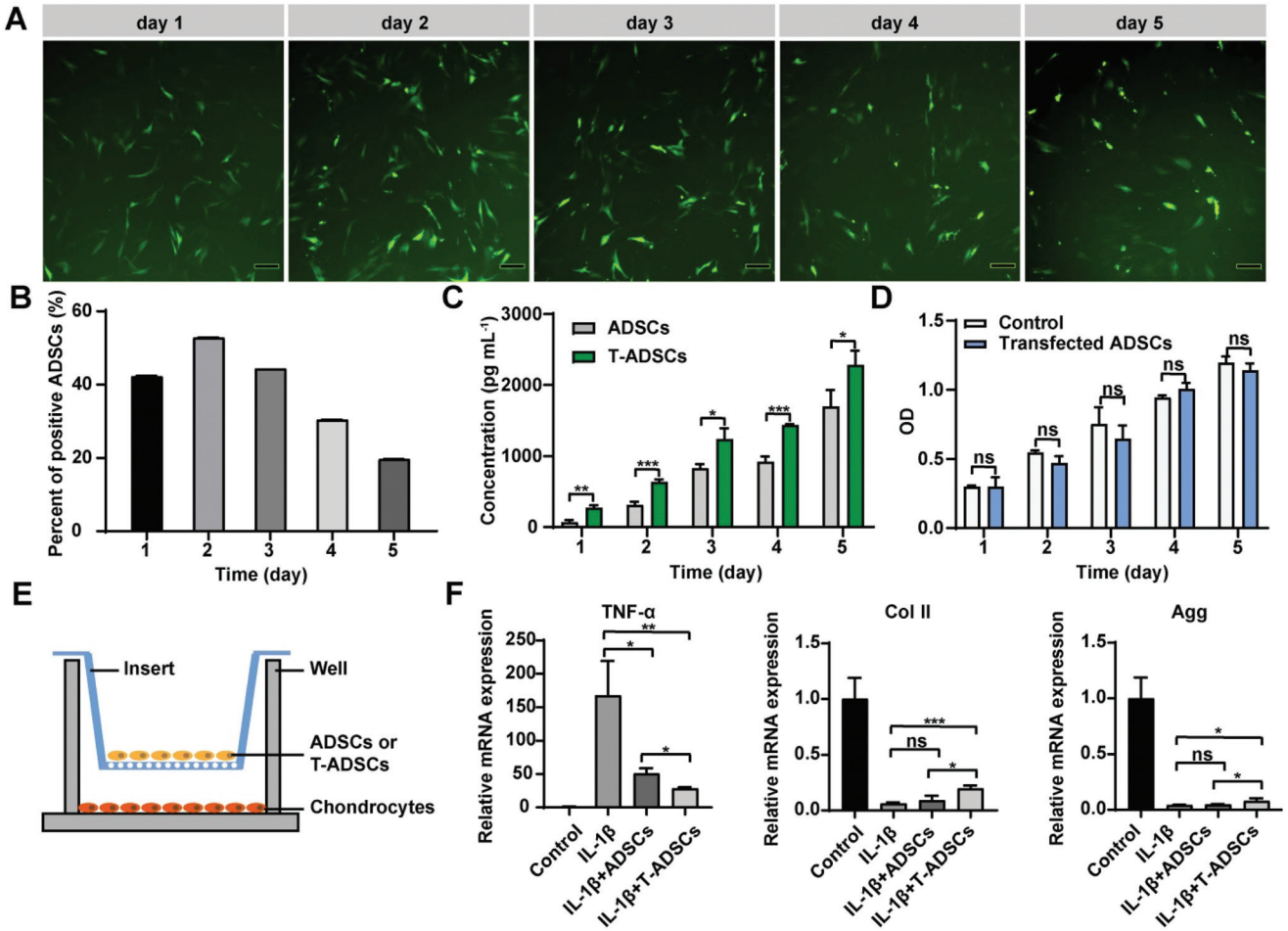

Fig. 4 Transfection of ADSCs and co-culture experiment. (A) EGFP expression in ADSCs transfected with PBAE/pEGFP-TGF-β1 nanocomplexes at a weight ratio of 60/1 lasted over time. Scale bar 200 μm. (B) Percentage of EGFP positive cells evaluated by flow cytometry, $n = 3$. (C) Cumulative concentrations of TGF-β1 in the ADSC and T-ADSC groups at different time points determined by ELISA. $n = 3$, $^{*}p < 0.05$, $^{**}p < 0.01$ and $^{***}p < 0.001$. (D) Cell proliferation test of ADSCs transfected with PBAE/pEGFP-TGF-β1 nanocomplexes at a weight ratio of 60/1; non-transfected ADSCs were used as the control. $n = 3$, ns represents $p > 0.05$. (E) The schematic illustration of the co-culture system. The insert contains chondrocytes, ADSCs or T-ADSCs, and the well contains chondrocytes. (F) qRT-PCR analysis of total RNA extracted from the chondrocytes in the wells on day 3 of the co-culture. $n = 3$, $^{*}p < 0.05$, $^{**}p < 0.01$ and $^{***}p < 0.001$. Data are presented as the mean ± standard deviation ($n = 3$).

II, an important indicator of the ECM protein,[38] showed a significant decrease in its expression in the PBS group (Fig. 5D). Interestingly, the group treated with the T-ADSC-loaded hydrogel presented a much stronger signal of Col II than the other groups in both the superficial and middle areas, exerting the best chondroprotective effect among the tested groups. As shown in Fig. 5E, compared to the PBS group, the other treatment groups demonstrated lower Mankin scores of articular cartilage. After hydrogel encapsulation, reduced Mankin scores were observed in the Gel + ADSC and Gel + T-ADSC treatment groups. T-ADSC-loaded hydrogel treatment resulted in the lowest Mankin score, highlighting its promising chondroprotective effect.

Anti-inflammatory effect of the T-ADSC-loaded hydrogel

As shown in Fig. 5F, the PBS group led to the presence of the highest amount of TNF-α in the synovial fluid. Treatment with the cells or cell-loaded hydrogels decreased the production of TNF-α. Compared to the unmodified ADSC group, the T-ADSCs enhanced the cellular function of anti-inflammation as evidenced by lower TNF-α production in the synovial fluid. Among all the treatment groups, the Gel + T-ADSC group showed the strongest anti-inflammatory effect, which significantly downregulated the TNF-α level by 62.1% compared to the PBS control. The H&E staining of the synovial joint tissue revealed that there were fewer inflammatory cells in the Gel + T-ADSC group (Fig. 6A), while an obvious infiltration of inflammatory cells was observed in the synovial joint tissue samples of the PBS control group. Fig. 6B shows that treatment with T-ADSCs, Gel + ADSCs, or Gel + T-ADSCs resulted in significantly reduced synovitis scores compared with the PBS control group. In comparison with the unmodified ADSCs, T-ADSC and Gel + ADSC treatment groups exhibited a lower synovitis score, suggesting an improved anti-inflammatory effect.

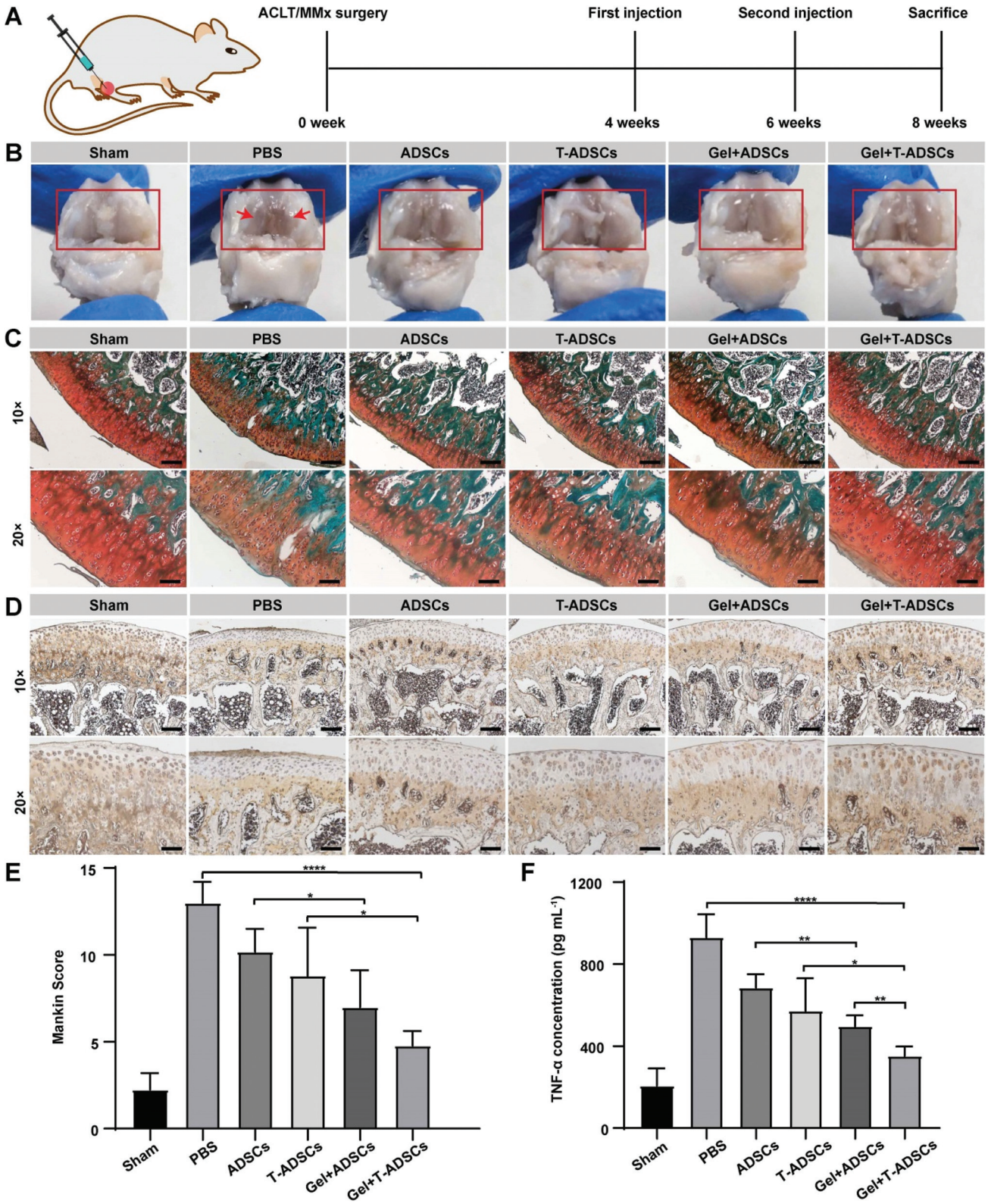

Fig. 5 Macroscopic and histological examination. (A) Graphical representation of the animal experimental design. (B) The gross appearance of the femur (red frames). Red arrow denotes cartilage degeneration. Histological analysis through (C) safranin O/fast green staining and (D) immunohistochemical staining of Col II. Scale bar of 10× images: 200 μm; scale bar of 20× images: 100 μm. (E) Mankin scores of tissue cross-sections. $n = 5$, *$p < 0.05$ and ****$p < 0.0001$. (F) The concentration of TNF-α in the synovial fluid collected from different treatment groups. $n = 5$, *$p < 0.05$, **$p < 0.01$ and ****$p < 0.0001$. Data are presented as the mean ± standard deviation ($n = 5$).

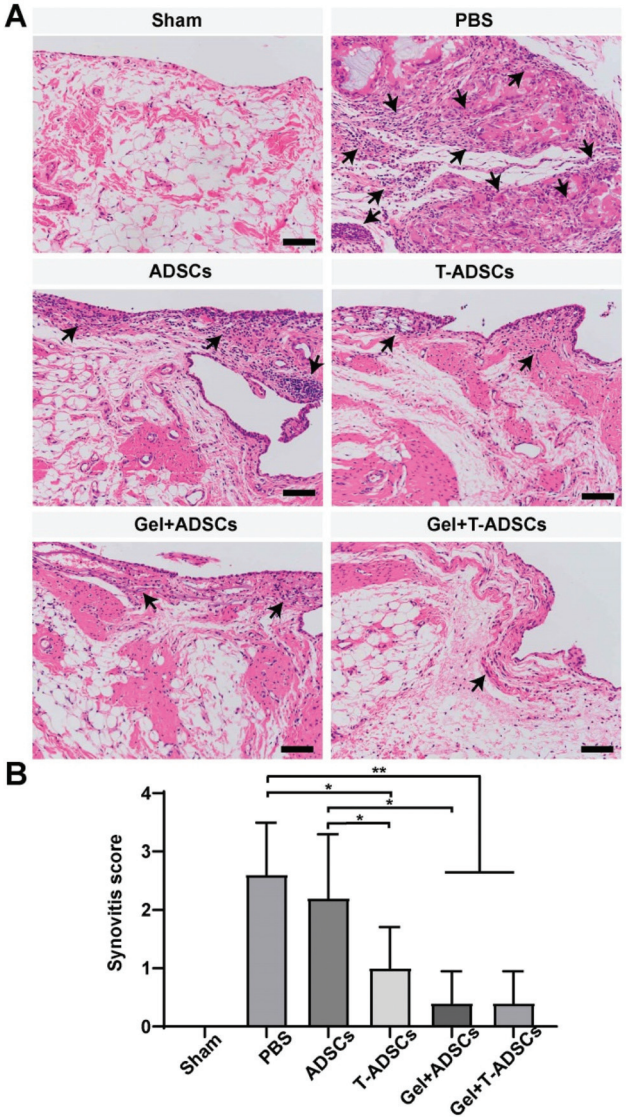

Fig. 6 Evaluation of synovitis. (A) H&E staining of the synovial joint tissue. Black arrows denote inflammatory cells. Scale bar 100 μm. (B) Synovitis scores of different groups based on the semi-quantitative evaluation of the three determining features of chronic synovitis: inflammatory infiltrates, synovial stroma and lining cell hyperplasia. Data are presented as the mean ± standard deviation (n = 5). *p < 0.05 and **p < 0.01.

Micro-CT

Severe bone erosion and cysts (red arrows) were observed in the PBS group after 4 weeks of treatment, whereas the cells or cell-loaded hydrogel groups showed a mild to moderate degree of bone erosion, loss, and cysts (Fig. 7A and B). ROI were selected to analyze the trabecular bone microstructure (Fig. 7C). An evident bone loss was generated in the PBS group. Compared to the sham group, the bone volume/tissue volume (BV/TV) of the tibia and femur in the PBS group decreased by 38.2% and 17.2%, respectively, and the trabecular number (Tb.N) decreased by 26.4% and 29.6% (Fig. 7D and E). However, after cells or cell-loaded hydrogel treatment, bone loss was relieved. The tibial BV/TV of the Gel + T-ADSC group was significantly higher than that of any other treatment group. The tibial and femoral Tb.N of the Gel + T-ADSC group was 28.6% and 42.1% higher than that of the PBS group, which was also higher than that of the other treatment groups. Taken together, the Gel + T-ADSC group exhibited the best therapeutic efficacy in preventing subchondral bone loss and structural destruction caused by the ACLT/MMx surgery.

Discussion

The intra-articular delivery of ADSCs is a promising therapy for OA treatment. Moreover, the therapeutic effects could be further enhanced by genetic modification of ADSCs to overexpress TGF-β1. However, direct injection of ADSCs leads to mechanical damage and poor retention of therapeutic cells.[39] Recently, ECM-mimicking hydrogels have shown enormous potential in cell-mediated tissue regeneration, including cartilage and muscle regeneration.[40,41] Herein, we delivered gene-engineered ADSCs within an ECM-mimicking hydrogel, which exhibited improved therapeutic outcomes of ADSCs for OA treatment.

HA, a linear polysaccharide consisting of alternating units of glucuronate and *N*-acetylglucosamine, is the main component of ECM in many tissues including cartilage, synovial, and connective tissues.[42] HA restores the viscoelastic properties of the synovial fluid and protects chondrocytes from apoptosis.[43,44] However, it lacks the ability to support cell adhesion.[45] As a major structural component of many tissues, Col I is able to self-assemble into collagen fibers in the physiological environment and provides cells with adhesion sites.[45] Thus, the incorporation of Col I into an HA-based injectable hydrogel simulates the ECM environment, serving as an ideal carrier for the intra-articular delivery of therapeutic cells. In the present study, we prepared an ECM-mimicking hydrogel *via* the self-crosslinking of HA-SH and self-assembly of Col I, which can be enzymatically or chemically degraded by reductants secreted in the physiological environment such as glutathione.[46–48] The hydrogel could be formed *in situ* under physiological conditions, and the formation of a disulfide bond and fibrillogenesis of Col I were accelerated when the pH of the precursor solution was slightly increased to 7.8.[49,50] The hydrogel precursor turned into a gel state within 6 minutes, allowing for the homogeneous encapsulation of ADSCs in the hydrogel without aggregation.[51]

The stiffness of the hydrogel is crucial for ADSC survival and growth, and the hydrogel matrix with a stiffness similar to the native microenvironment is favorable. Therefore, hydrogels with different stiffness rates were screened in the 3D culture study of ADSCs, which were encapsulated within the hydrogel matrix to evaluate the cytocompatibility. The 4-HA-Col matrix with the highest stiffness (over 1 kPa) among the candidate hydrogels resulted in the unchanged round morphology of ADSCs during the culture period. However, the cells exhibited

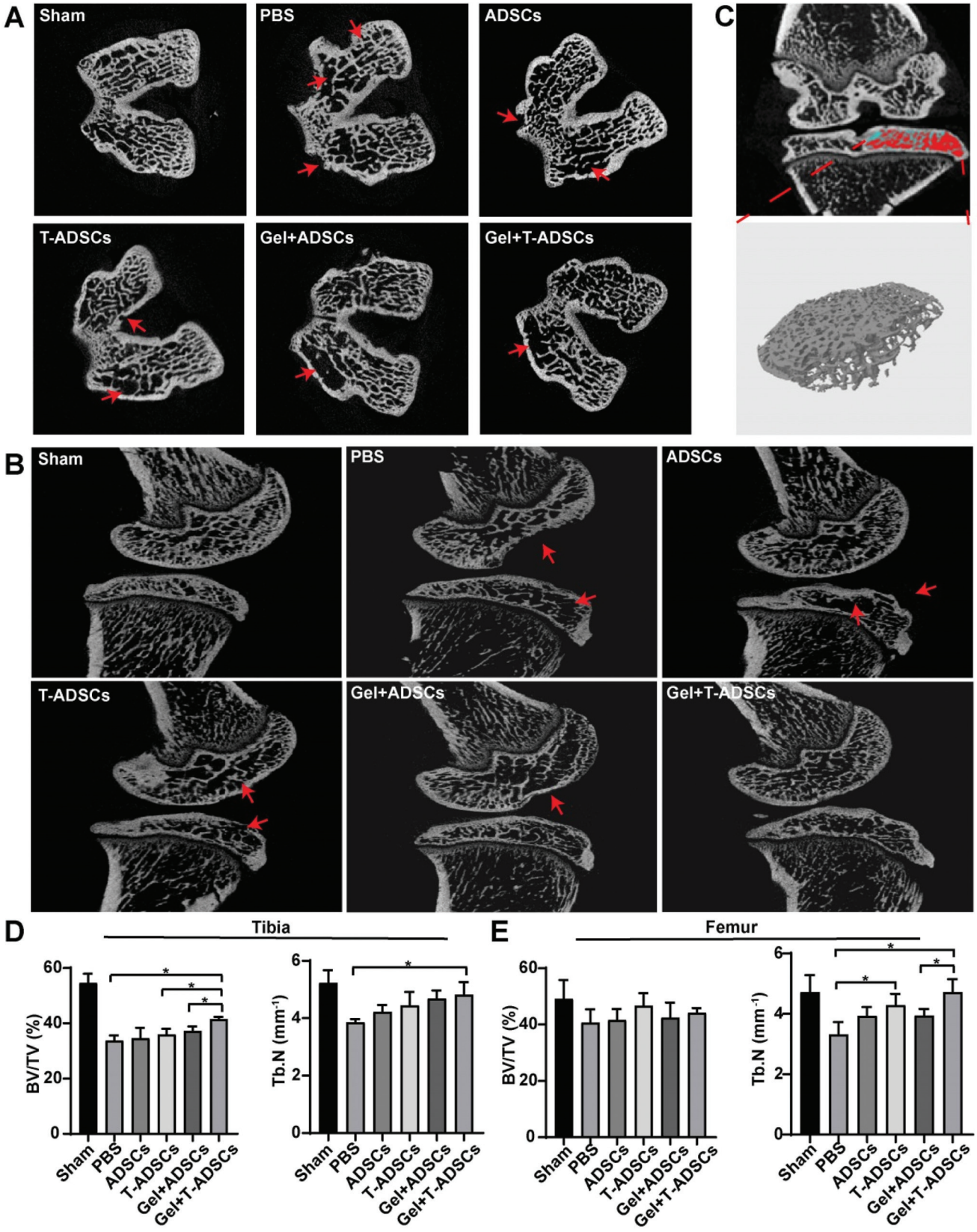

Fig. 7 Micro-CT analysis of different treatment groups. (A) Representative images of the femoral axial section of different treatment groups. (B) Representative images of the sagittal sections of the whole keen joint of different treatment groups. Red arrows denote bone erosion, loss, and cysts. (C) Representative images of the ROI used for the analysis of the trabecular bone microstructure. (D and E) The BV/TV and Tb.N of the trabecular bone. Data are presented as the mean ± standard deviation (n = 3). *p < 0.05.

elongated, well-spread, and interconnected morphology when cultured in the relatively softer 2-HA-Col hydrogel. Additionally, 2-HA-Col exhibited shear-thinning properties, which enabled cell delivery through the minimally invasive approach of injection,[52] while maintaining cell viability of up to 97% during this process. Taken together, the 2-HA-Col hydrogel was selected as the carrier for the intra-articular delivery of ADSCs.

For the genetic engineering of ADSCs, the optimal nanocomplex formulation was screened and identified, which exhibited a favorable transfection efficiency and cytocompatibility on ADSCs. Meanwhile, the constant and increased expression of TGF-β1 lasting up to 5 days was detected in T-ADSCs. These results indicated that gene modification with the optimal PBAE/pEGFP-TGF-β1 nanocomplexes endowed ADSCs with enhanced paracrine effects.

To investigate the impact of T-ADSCs on OA-like chondrocytes, a co-culture system was established to mimic the *in vivo* interaction between therapeutic cells and OA-like chondrocytes. Pro-inflammatory cytokines secreted by synovial tissues, chondrocytes, mononuclear cells, and osteolast, such as TNF-α and IL-1β, could upregulate the production of catabolic factors in OA miroenvironment, leading to the degradation of cartilage.[53] Therefore, the level of proinflammatory cytokines secreted by OA-like chondrocytes was evaluated. Consistent with the results reported in a previous study, the treatment of ADSCs decreased the expression of TNF-α in OA-like chondrocytes.[36] As expected, a significantly more potent anti-inflammatory effect was observed following the treatment of T-ADSCs than ADSCs. This could be attributed to the enhanced expression of TGF-β1 that effectively alleviated the proinflammatory state of OA-like chondrocytes resulted from IL-1β stimulation.[54] Please note that the *in vitro* experiments were performed in triplicate, which might be a limitation for statistical evaluation. We will further increase the number of replicates to validate the statistical significance during future preclinical development.

Finally, the *in vivo* therapeutic effect of the ECM-mimicking hydrogel carrying T-ADSCs was evaluated on a surgically induced rat OA model which has been commonly used in OA research. A previous study demonstrated that ADSCs could decrease TNF-α production in the synovial fluid, thereby reducing joint inflammation.[55] Herein, the content of TNF-α in the synovial fluid was quantified to evaluate the *in vivo* anti-inflammatory effect of different treatment groups. A lower expression of TNF-α was detected in the T-ADSC group than in the ADSC group, and encapsulation of ADSCs or T-ADSCs within the hydrogel further inhibited TNF-α production. The optimal anti-inflammatory effect of Gel + ADSC treatment was validated by the lowest expression of TNF-α in the synovial fluid. The histological examination revealed the highest content of proteoglycans and Col II in the cartilage following the treatment of the T-ADSC-loaded hydrogel, highlighting its potential protective effects on cartilage. Meanwhile, the remarkable chondroprotective and anti-inflammatory effects following T-ADSC-loaded hydrogel treatment in turn contributed to the reduction on subchondral bone loss and destruction. The favorable therapeutic benefits from the T-ADSC-loaded hydrogel were likely attributed to the following aspects: (1) the ECM-mimicking hydrogel provided desirable structural support and protection for cells during and post-implantation, thereby maintaining the cell viability; and (2) the gene-engineered ADSCs that overexpressed TGF-β1 were endowed with the enhanced paracrine chondroprotective effects by increasing the expression of the ECM proteins and decreasing the production of proinflammatory cytokines, which improved the therapeutic efficacy.

Conclusions

In summary, we successfully developed an ECM-mimicking hydrogel incorporating the gene-engineered ADSCs, and investigated its potent therapeutic effects for OA treatment. The yielded injectable hydrogel served as an ideal carrier for cell delivery with excellent cytocompatibility and protective effects. Meanwhile, ADSCs were successfully engineered to overexpress TGF-β1 through nanocomplex-mediated transfection, and the resulted T-ADSCs showed an enhanced paracrine effect on OA-like chondrocytes. In a surgically induced rat OA model, the intra-articular injection of the T-ADSC-loaded hydrogel significantly alleviated cartilage degeneration, joint inflammation, subchondral bone loss, and structure destruction. Overall, this study provides a promising strategy to synergistically improve the therapeutic effects of ADSCs for OA treatment by delivering genetically modified ADSCs that overexpress TGF-β1 within an ECM-mimicking hydrogel.

Author contributions

Wei Yu: methodology, investigation, data analysis, and writing – original draft. Bin Hu: investigation, data analysis, and writing – review and editing. Kofi Oti Boakye-Yiadom: writing – review and editing. William Ho: writing – review and editing. Qijing Chen: methodology and data analysis. Xiaoyang Xu: conceptualization, supervision, data analysis, funding acquisition, methodology, and writing – review and editing. Xue-Qing Zhang: conceptualization, supervision, data analysis, funding acquisition, methodology, and writing – original draft, review and editing. All authors have given approval for the final version of the manuscript.

Conflicts of interest

There are no conflicts to declare.

Acknowledgements

X. Zhang acknowledges the financial support from the Interdisciplinary Program of Shanghai Jiao Tong University (project number ZH2018ZDA36 (19X190020006)), the

Shanghai Jiao Tong University Scientific and Technological Innovation Funds (2019TPA10), and the Foundation of National Facility for Translational Medicine (Shanghai) (TMSK-2020-008). X. X. acknowledges the support from the American Heart Association (19AIREA34380849) and the National Science Foundation (2001606).

References

1 Y. Liu, A. Jackson and S. Cosgrove, *Osteoarthr. Cartil.*, 2009, **17**, 1333–1340.
2 K. Sinusas, *Am. Fam. Physician*, 2012, **85**, 49–56.
3 A. D. Woolf and B. Pfleger, *Bull. W. H. O.*, 2003, **81**, 646–656.
4 R. Liu-Bryan and R. Terkeltaub, *Nat. Rev. Rheumatol.*, 2015, **11**, 35–44.
5 M. Bhattacharjee, J. L. E. Ivirico, H.-M. Kan, R. Bordett, R. Pandey, T. Otsuka, L. S. Nair and C. T. Laurencin, *Sci. Rep.*, 2020, **10**, 1–15.
6 L.-B. Jiang, S. Lee, Y. Wang, Q.-T. Xu, D.-H. Meng and J. Zhang, *Osteoarthr. Cartil.*, 2016, **24**, 1071–1081.
7 C. Manferdini, M. Maumus, E. Gabusi, A. Piacentini, G. Filardo, J. A. Peyrafitte, C. Jorgensen, P. Bourin, S. Fleury-Cappellesso and A. Facchini, *Arthritis Rheum.*, 2013, **65**, 1271–1281.
8 M. Maumus, C. Manferdini, K. Toupet, J.-A. Peyrafitte, R. Ferreira, A. Facchini, E. Gabusi, P. Bourin, C. Jorgensen and G. Lisignoli, *Stem Cell Res.*, 2013, **11**, 834–844.
9 H. Jung, H. H. Kim, D. H. Lee, Y.-S. Hwang, H.-C. Yang and J.-C. Park, *Cytotechnology*, 2011, **63**, 57–66.
10 E. D. Ahmadi, T. I. Raja, S. A. Khaghani, C. F. Soon, M. Mozafari, M. Youseffi and F. Sefat, *Mater. Today: Proc.*, 2018, **5**, 15540–15549.
11 E. B. Davidson, P. Van der Kraan and W. Van Den Berg, *Osteoarthr. Cartil.*, 2007, **15**, 597–604.
12 H. Lee, H. Kim, J. Seo, K. Choi, Y. Lee, K. Park, S. Kim, A. Mobasheri and H. Choi, *Inflammopharmacology*, 2020, **28**, 1237–1252.
13 E. A. Silva, E.-S. Kim, H. J. Kong and D. J. Mooney, *Proc. Natl. Acad. Sci. U. S. A.*, 2008, **105**, 14347–14352.
14 Y. Wang, X. He, K. F. Bruggeman, B. Gayen, A. Tricoli, W. M. Lee, R. J. Williams and D. R. Nisbet, *Adv. Funct. Mater.*, 2020, **30**, 1900390.
15 Z. Tang, F. Jiang, Y. Zhang, Y. Zhang, X. Huang, Y. Wang, D. Zhang, N. Ni, F. Liu and M. Luo, *Biomaterials*, 2019, **194**, 57–72.
16 M. W. Tibbitt and K. S. Anseth, *Biotechnol. Bioeng.*, 2009, **103**, 655–663.
17 K. T. Nguyen and J. L. West, *Biomaterials*, 2002, **23**, 4307–4314.
18 A. P. Mathew, S. Uthaman, K.-H. Cho, C.-S. Cho and I.-K. Park, *Int. J. Biol. Macromol.*, 2018, **110**, 17–29.
19 J. Wu, Q. Chen, C. Deng, B. Xu, Z. Zhang, Y. Yang and T. Lu, *Theranostics*, 2020, **10**, 9843–9864.
20 H. Zhou, C. Liang, Z. Wei, Y. Bai, S. B. Bhaduri, T. J. Webster, L. Bian and L. Yang, *Mater. Today*, 2019, **28**, 81–97.
21 Z. Yuan, Y.-H. Tsou, X.-Q. Zhang, S. Huang, Y. Yang, M. Gao, W. Ho, Q. Zhao, X. Ye and X. Xu, *ACS Appl. Mater. Interfaces*, 2019, **11**, 38429–38439.
22 Y. Dong, A. O. Saeed, W. Hassan, C. Keigher, Y. Zheng, H. Tai, A. Pandit and W. Wang, *Macromol. Rapid Commun.*, 2012, **33**, 120–126.
23 B. A. Bunnell, M. Flaat, C. Gagliardi, B. Patel and C. Ripoll, *Methods*, 2008, **45**, 115–120.
24 C. Lorenzo, G. Pérez-Chacón, G. Garaulet, Z. Mallorquín, J. M. Zapata and A. Rodríguez, *Cancer Gene Ther.*, 2015, **22**, 542–551.
25 T. T. Smith, S. B. Stephan, H. F. Moffett, L. E. McKnight, W. Ji, D. Reiman, E. Bonagofski, M. E. Wohlfahrt, S. P. Pillai and M. T. Stephan, *Nat. Nanotechnol.*, 2017, **12**, 813–820.
26 K. Chen, Y. Yan, C. Li, J. Yuan, F. Wang, P. Huang, N. Qian, J. Qi, H. Zhou and Q. Zhou, *Cell Death Dis.*, 2017, **8**, e3109.
27 Z. Qiao, J. Tang, W. Wu, J. Tang and M. Liu, *BMC Complementary Altern. Med.*, 2019, **19**, 1–8.
28 Y. Shi, X. Hu, J. Cheng, X. Zhang, F. Zhao, W. Shi, B. Ren, H. Yu, P. Yang and Z. Li, *Nat. Commun.*, 2019, **10**, 1–14.
29 T. Hayami, M. Pickarski, Y. Zhuo, G. A. Wesolowski, G. A. Rodan and L. T. Duong, *Bone*, 2006, **38**, 234–243.
30 H. R. Moody, B. J. Heard, C. B. Frank, N. G. Shrive and A. O. Oloyede, *J. Anat.*, 2012, **221**, 47–54.
31 V. Krenn, L. Morawietz, T. Häupl, J. Neidel, I. Petersen and A. König, *Pathol., Res. Pract.*, 2002, **198**, 317–325.
32 Y. Chen, J. Sui, Q. Wang, Y. Yin, J. Liu, Q. Wang, X. Han, Y. Sun, Y. Fan and X. Zhang, *Carbohydr. Polym.*, 2018, **190**, 57–66.
33 G. L. Ellman, K. D. Courtney, V. Andres Jr. and R. M. Featherstone, *Biochem. Pharmacol.*, 1961, **7**, 88–95.
34 X. Z. Shu, Y. Liu, Y. Luo, M. C. Roberts and G. D. Prestwich, *Biomacromolecules*, 2002, **3**, 1304–1311.
35 M. Guvendiren, H. D. Lu and J. A. Burdick, *Soft Matter*, 2012, **8**, 260–272.
36 L. Mei, B. Shen, P. Ling, S. Liu, J. Xue, F. Liu, H. Shao, J. Chen, A. Ma and X. Liu, *PLoS One*, 2017, **12**, e0176107.
37 A. Schäffler and C. Büchler, *Stem Cells*, 2007, **25**, 818–827.
38 Y. Xu, Y. Gu, F. Cai, K. Xi, T. Xin, J. Tang, L. Wu, Z. Wang, F. Wang and L. Deng, *Adv. Funct. Mater.*, 2020, **30**, 2006333.
39 L. Cai, R. E. Dewi and S. C. Heilshorn, *Adv. Funct. Mater.*, 2015, **25**, 1344–1351.
40 Y. Yao, P. Wang, X. Li, Y. Xu, G. Lu, Q. Jiang, Y. Sun, Y. Fan and X. Zhang, *Acta Biomater.*, 2020, **111**, 197–207.
41 Y. Xu, X. Chen, Y. Qian, H. Tang, J. Song, X. Qu, B. Yue and W. E. Yuan, *Adv. Funct. Mater.*, 2020, **30**, 2002378.
42 M. Shafiq, Y. Jung and S. H. Kim, *Biomaterials*, 2016, **90**, 85–115.
43 R. D. Altman, A. Manjoo, A. Fierlinger, F. Niazi and M. Nicholls, *BMC Musculoskeletal Disord.*, 2015, **16**, 1–10.
44 P. Wehling, C. Evans, J. Wehling and W. Maixner, *Ther. Adv. Musculoskeletal Dis.*, 2017, **9**, 183–196.

45 S. R. Caliari and J. A. Burdick, *Nat. Methods*, 2016, **13**, 405–414.
46 M. Kar, Y.-R. V. Shih, D. O. Velez, P. Cabrales and S. Varghese, *Biomaterials*, 2016, **77**, 186–197.
47 S.-Y. Choh, D. Cross and C. Wang, *Biomacromolecules*, 2011, **12**, 1126–1136.
48 J. Zhang, A. Skardal and G. D. Prestwich, *Biomaterials*, 2008, **29**, 4521–4531.
49 D. Bermejo-Velasco, A. Azémar, O. P. Oommen, J. N. Hilborn and O. P. Varghese, *Biomacromolecules*, 2019, **20**, 1412–1420.
50 T. Walimbe, S. Calve, A. Panitch and M. P. Sivasankar, *Acta Biomater.*, 2019, **87**, 97–107.
51 K. Gwon, E. Kim and G. Tae, *Acta Biomater.*, 2017, **49**, 284–295.
52 H. Wang, D. Zhu, A. Paul, L. Cai, A. Enejder, F. Yang and S. C. Heilshorn, *Adv. Funct. Mater.*, 2017, **27**, 1605609.
53 M. Kapoor, J. Martel-Pelletier, D. Lajeunesse, J.-P. Pelletier and H. Fahmi, *Nat. Rev. Rheumatol.*, 2011, **7**, 33–42.
54 H. Van Beuningen, P. Van der Kraan, V. D. O. Arntz and W. Van Den Berg, *Ann. Rheum. Dis.*, 1993, **52**, 185–191.
55 L. Mei, B. Shen, J. Xue, S. Liu, A. Ma, F. Liu, H. Shao, J. Chen, Q. Chen and F. Liu, *Biochem. Biophys. Res. Commun.*, 2017, **494**, 285–291.